A comparison of SuperDARN ACF fitting methods

A. J. Ribeiro,[1] J. M. Ruohoniemi,[1] P. V. Ponomarenko,[1,2] L. B. N. Clausen,[3] J. B. H. Baker,[1] R. A. Greenwald,[1] K. Oksavik,[4,5] and S. de Larquier[1]

[1]   The Super Dual Auroral Radar Network (SuperDARN) is a worldwide chain of HF radars which monitor plasma dynamics in the ionosphere. Autocorrelation functions are routinely calculated from the radar returns and applied to estimate Doppler velocity, spectral width, and backscatter power. This fitting has traditionally been performed by a routine called FITACF. This routine initiates a fitting by selecting a subset of valid phase measurements and then empirically adjusting for 2π phase ambiguities. The slope of the phase variation with lag time then provides Doppler velocity. Doppler spectral width is found by an independent fitting of the decay of power to an assumed exponential or Gaussian function. In this paper, we use simulated data to assess the performance of FITACF, as well as two other newer fitting techniques, named FITEX2 and LMFIT. The key new feature of FITEX2 is that phase models are compared in a least-squares fitting sense with the actual data phases to determine the best fit, eliminating some ambiguities which are present in FITACF. The key new feature of LMFIT is that the complex autocorrelation function (ACF) itself is fit, and Doppler velocity, spectral width, and backscatter power are solved simultaneously. We discuss some of the issues that negatively impact FITACF and find that of the algorithms tested, LMFIT provides the best overall performance in fitting the SuperDARN ACFs. The techniques and the data simulator are applicable to other radar systems that utilize multipulse sequences to make simultaneous range and velocity determinations under aliasing conditions.

1.   Introduction

[2]   The Super Dual Auroral Radar Network (Super-DARN) is a chain of HF radars which monitor ionospheric plasma convection in the northern and southern hemispheres by detecting backscatter from ionospheric plasma irregularities [*Greenwald et al.*, 1985; *Chisham et al.*, 2007]. A typical SuperDARN radar has 16 look directions ("beams") separated by 3.24° in azimuth, with 75–100 range gates along each beam separated by 45 km. The dwell time on any particular beam is typically 3–7 s (integration period) which results in a 1–2 min azimuthal scan. Examples of field of view plots of a single scan are shown in Figure 1. Figure 1a shows signal-to-noise ratio (SNR) ("backscattered power"),

Figure 1b shows Doppler velocity, and Figure 1c shows Doppler spectral width. These data are fairly representative in displaying a range of echo types including (1) an extended region of low-velocity ground scatter at greater ranges on the more westward beams, (2) meteor wind scatter at the very near ranges, (3) a high-velocity ionospheric scatter feature on the middle beams, and (4) spotty noise/interference elsewhere but especially on the more northward beams.

[3]   The nature of the primary targets detected by SuperDARN radars introduces certain complications. The principal dilemma arises because the radar was designed to detect targets with Doppler velocities of up to 2 km/s out to a range of 4500 km. These conditions impose mutually exclusive requirements on the nominal pulse repetition frequency (PRF). To avoid ambiguities in range, we require a long interpulse period (PRF $\leq$ 33.3 Hz), while to avoid ambiguities in Doppler velocity, we must have a shirt interpulse period (PRF $\geq$ 320 Hz). Some techniques which have been used to solve this problem are complementary codes, alternating codes [*Lehtinen*, 1986], and aperiodic sequences [*Uppala and Sahr*, 1994]. In order to resolve this dilemma, the radars employ multipulse sequences to simultaneously determine the range and Doppler velocity of targets [*Farley*, 1972; *Greenwald et al.*, 1985; *Hanuise et al.*, 1993; *Baker et al.*, 1995; *Barthes et al.*, 1998; *Ponomarenko and Waters*, 2006]. This means that instead of transmitting solitary pulses that are separated by a fixed time determined by

[1]The Bradley Department of Electrical and Computer Engineering, Virginia Tech, Blacksburg, Virginia, USA.
[2]Institute of Space and Atmospheric Studies, University of Saskatchewan, Saskatoon, Saskatchewan, Canada.
[3]Institute for Geophysics and Extraterrestrial Physics, TU Braunschweig, Braunschweig, Germany.
[4]Department of Physics and Technology, University of Bergen, Bergen, Norway.
[5]Birkeland Centre for Space Science, Bergen, Norway.

Corresponding author: A. J. Ribeiro, 1901 Innovation Dr, Suite 1033, Blacksburg, VA 24060, USA. (ribeiro@vt.edu)
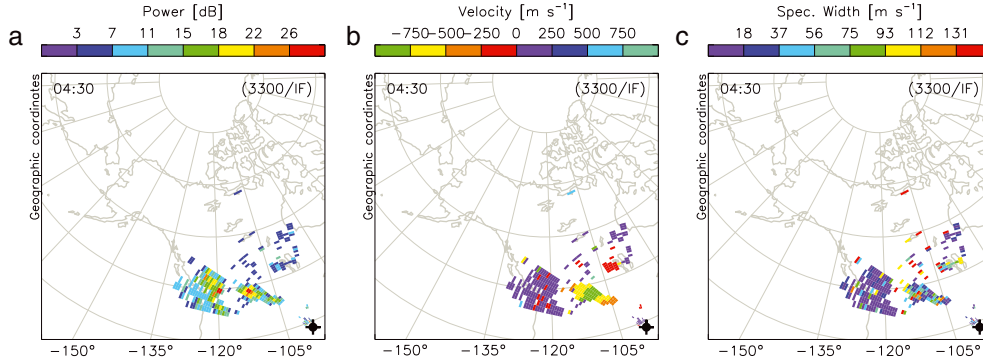
Figure 1. Examples of SuperDARN radar field of view plots. The data were collected with the Fort Hays West radar on 10 September 2011 over the interval 04:30–04:31 UT. The radar, located at 38.86°N, –99.39°W, was scanning across 22 beam directions, with range gates beginning at 180 km. The data were solved using FITEX2 as described in the text. The panels show (a) backscatter power, (b) Doppler velocity, and (c) Doppler spectral width.

the PRF, the radars periodically emit sequences of pulses that are separated unevenly in time by integer multipliers of an "elementary lag time" τ_0 =1.5–2.4 ms. By sampling the returns from a fixed range for each pulse of the sequence using a coherent receiver, all products of the complex autocorrelation function (ACF), $R_k = V(t)V^*(t + k\tau_0)$, where V is the receiver voltage sample and k is the lag number, can be calculated from 0 to $n\tau_0$, where n is the number of lags, with occasional misses at certain lags. An ACF is calculated for each range gate from the returns from each multipulse sequence. Averaging the returns over multiple sequence transmissions partially suppresses the contributions from pulses that encounter other scattering regions at the same sampling times (cross-range interference, CRI, a type of clutter) [*Baker et al.*, 1995]. This averaging occurs within what is called an integration period. An example of a standard SuperDARN multipulse sequence is shown in Figure 2. One observes that with this eight pulse sequence, all but two of the lags can be computed up to a lag of 24.

[4] An integration period is typically 3–7 s in length. The total number of multipulse sequences transmitted during an integration varies between about 15 and 60. The ACFs calculated from all the sequences are then integrated in order to minimize interference and increase gain. The integrated ACFs are fit to model functions in order to resolve Doppler velocity (v), spectral width (w), and backscatter power (signal-to-noise ratio, SNR) as functions of range. Figure 3a shows an ACF from the Fort Hays West radar taken from the period of Figure 1. The ACF consists of a real part (red curve), $Re\{R\}$, and an imaginary part (blue curve), $Im\{R\}$, in quadrature. Note that the real part has a maximum at lag zero, and the imaginary part has a value of zero at lag zero. The Doppler shift imposed on the frequency of the returned signal is manifested as a systematic variation of phase with lag. The phase ϕ at lag τ is calculated as $\phi(\tau) = \arctan(Im\{R(\tau)\}/Re\{R(\tau)\})$. Figure 3b illustrates the variation of phase with lag for the ACF of Figure 3a. The maximum Doppler frequency shift, f_{dmax}, that can be resolved is related to the basic lag time, τ_0, by $f_{dmax} = 1/(2\tau_0)$. Typically, this value is $\approx$ 300 Hz, corresponding to a maximum Doppler velocity of $\approx$ 4000 m/s. The lag power P at lag τ is calculated as $P(\tau) = |R(\tau)|$.

The SNR is found using the fitted signal level at lag zero, R_0, of the ACF. The spectral width is obtained as a decay of the amplitude of the ACF with lag, i.e., a decrease in $P(\tau)$ with τ. Figure 3c shows the lag powers for the ACF of Figure 3a. A detailed discussion of the physical significicance of spectral width in terms of signal composition is given by *Ponomarenko and Waters* [2006]. In order to actually calculate v, w, and SNR from the radar data, fits must be performed to the lag phases and powers of the ACFs.

[5] FITACF is the name of the traditional routine used to process SuperDARN ACFs. While it has performed reasonably well since the inception of SuperDARN, its performance has rarely been tested, mainly because of the absence of a realistic data simulator accounting for both regular and random components of the backscatter echoes. Some other algorithms have been developed over the last few years that attempt to improve data quality but to compare their performance to that of FITACF objectively; again, one needs to have a controlled set of inputs such as can be provided by a
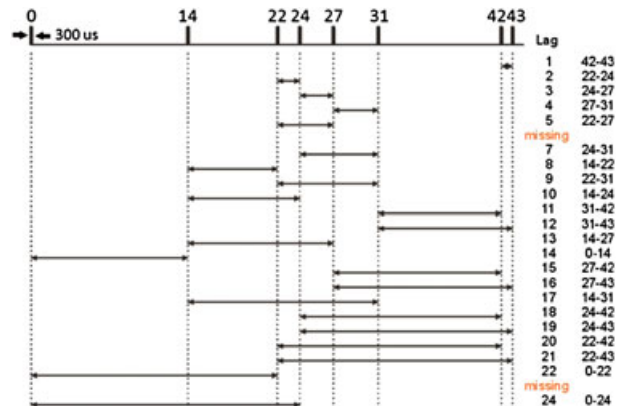
Figure 2. An illustration of a standard SuperDARN pulse sequence, called *katscan*. The raised bars represent transmit pulses, and the numbers represent lag time from the first pulse until transmission. The pulse duration is 300 μs, and the basic lag time is typically either 1500 or 2400 μs. Samples are recorded in between transmit pulses and after the last pulse. (Figure courtesy of K. A. McWilliams)
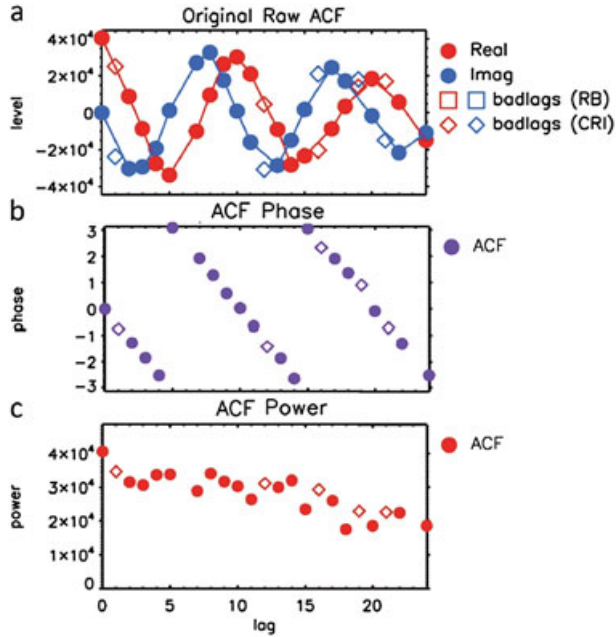
Figure 3. (a) A SuperDARN ACF from the Fort Hays West radar in Kansas. The data were collected on 10 September 2011 at 04:30 UT from beam 7 and range gate 27. The real part of the ACF is plotted in red, and the imaginary part is plotted in blue. The ACF values at individual lags are plotted as discrete points. Any lags that have been identified as bad are plotted as open shapes. (b) The lag phases in radians for the ACF in Figure 3a. (c) The lag powers for the ACF in Figure 3a.

comprehensive data simulator. An appropriate simulator has recently been developed by *Ribeiro et al.* [2013] based on the collective scatter model initially conceived by *Ponomarenko et al.* [2008].

[6] In this paper, we examine three different ways of extracting Doppler velocity, spectral width, and SNR from SuperDARN ACFs. We first analyze the conventional FITACF package, in use for almost 30 years. The second method is FITEX2, which is an iteration on a routine called FITEX, which was developed in order to fit a specific multipulse sequence. Finally, we test so-called LMFIT, which uses the Levenberg-Marquardt algorithm [*Levenberg*, 1944; *Marquardt*, 1963] to fit the complex ACF in a single procedure. The aim of this analysis is to compare the performances of the three routines and determine which is the most reliable at extracting Doppler velocity and spectral width from SuperDARN ACFs.

2. Description of Fitting Methods

2.1. Common Routines

[7] Some procedures are common to all three ACF fitting routines. This includes subroutines which determine so-called "bad" lags, which are not suitable for use in the fitting process. A lag is flagged as bad in initial processing if it is (1) contaminated by CRI, or, (2) affected by transmitter pulse overlap (a pulse was being transmitted when a sample should have been recorded). All three fitting methods use the same such subroutines in initial processing and therefore

have the same lags flagged as bad. A "good" lag is one which is not bad, and a minimum of four good lags must be present for fitting to occur. In Figure 3a, lags that have been identified as bad in initial processing are plotted as open circles and diamonds. Additionally, all three routines use the same algorithms to find a noise power level, *N*, for each integration period, which is done by calculating the average *P*(0) of the 10 lowest power ACFs on a given beam sounding. The three routines will not have the same exact noise figure, however, because FITACF does some calculations with integers, whereas FITEX2 and LMFIT use double precision numbers for all calculations.

2.2. FITACF

[8] FITACF is the traditional method used for fitting SuperDARN ACFs. The version used in this paper is distributed with the SuperDARN Radar Software Toolkit 3 [1]. In addition to the three common routines discussed previously, another bad lag routine is also invoked by FITACF at the stage of fitting the ACF. This routine identifies additional lags as bad depending on some empirical criteria for a single Doppler component (e.g., monotonous power decay with increasing lags) [*Ponomarenko and Waters*, 2006]. This routine is not used in the other two fitting routines because of recommendations made by P. Ponomarenko and C. Waters at the 2006 SuperDARN meeting held at Chincoteague, Virginia. However, in FITEX2 and LMFIT, any lags with power values less than the statistical fluctuation level ($\sigma_P = P(0)/\sqrt{N_{\mathrm{avg}}}$, where N_{avg} is the number of integrated pulse sequences) are assigned a very low weight, so as to be effectively excluded from the fitting, in accordance with the same recommendations. Lags flagged as bad by this checking are indicated by open triangles in plots of the type shown in Figure 3.

[9] To resolve all three major information parameters, *v*, *w*, and SNR, FITACF applies two separate fitting procedures. The Doppler velocity is determined from the variation of phase with lag, i.e.,

$$v = \frac{\lambda}{4\pi} \frac{\partial \phi}{\partial \tau}, \qquad (1)$$

where λ is the radar wavelength. A linear least-squares fit is performed to determine $\delta\phi/\delta\tau$. In determining the phase slope, it is important to account for the 2π uncertainty in the phase shift variation with τ. With FITACF, an initial estimate of the number of 2π phase cycles across the full extent of lag time is made using the phases of the first four lags. Subsequent lags are fit by advancing one lag at a time and considering whether to unfold a 2π phase variation and then fitting the phase slope over the augmented set of lags. The fact that FITACF must make an initial guess will be an important issue later in this discussion.

[10] A completed FITACF phase-fit for the data shown in Figure 3 is shown in Figure 4a. The phases corresponding to the data are plotted in purple, while the fitted solution is plotted as a green dash-dotted line. The solid circles and open diamonds represent the "good" and "bad" lags, respectively. The Doppler velocity is calculated from the slope of the best-fit line. Note that even though the data and fit are shown as a sawtooth pattern, the fitting is actually performed

---

[1]http://superdarn.jhuapl.edu/software/index.html
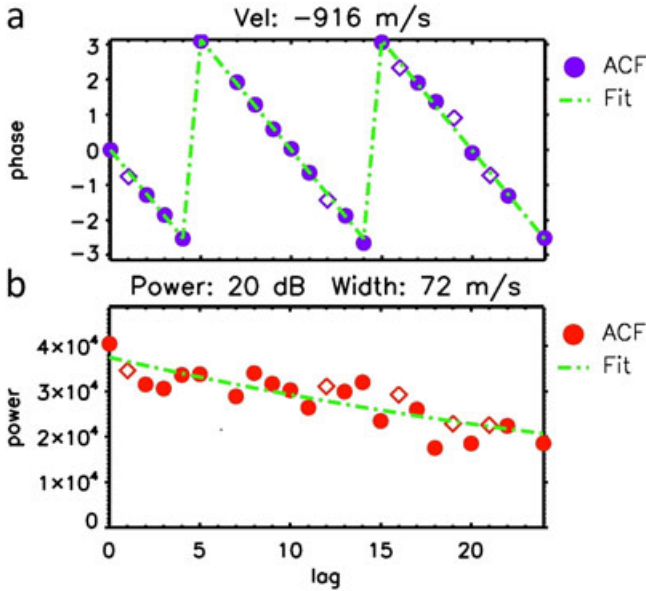
Figure 4. FITACF results for the data in Figure 3. (a) The phase fit used to resolve Doppler velocity. The actual lag phases are plotted in purple, and the fit is plotted in green. (b) Log power fit used to resolve power (SNR) and spectral width. The actual lag powers are plotted in red, and the fit is plotted in green.

as a straight line that extends over multiple 2π ranges. In this case, the line-of-sight Doppler velocity calculated from the slope of the best-fit line is $v = -916$ m/s, where the minus signifies motion away from the radar.

[11] In order to resolve Doppler spectral width and power, a model is fitted to $|R(\tau)|$. For the entirety of this paper, we will assume that the ACF amplitude decays exponentially, i.e., $|R(\tau)| = R_0 e^{-\tau/t_d}$ where t_d is a decay time constant [*Ponomarenko et al.*, 2007]. For the actual calculation of parameters, a second linear least-squares fit is performed to the natural logarithm of the $|R(\tau)|$ of the ACF.

[12] The resulting y-intercept of the fitted model represents the fitted lag zero power, R_0, which is then used to calculate SNR in dB,

$$\text{SNR} = 10 \log_{10}(R_0/N). \qquad (2)$$

[13] The slope of the linear log-power fit is used to calculate the exponential decay time of the signal, which in turn is used to find the spectral width of the ACF, which is determined as the width of a model spectrum at a half-power level and for the exponential model can be expressed as

$$w = \frac{\lambda}{2\pi t_d}. \qquad (3)$$

[14] A completed log-power fit is shown in Figure 4b. The lag powers are presented as red symbols, while the best fit line is plotted in green. For this particular ACF, the FITACF analysis gives $w = 72$ m/s and an SNR= 20 dB.
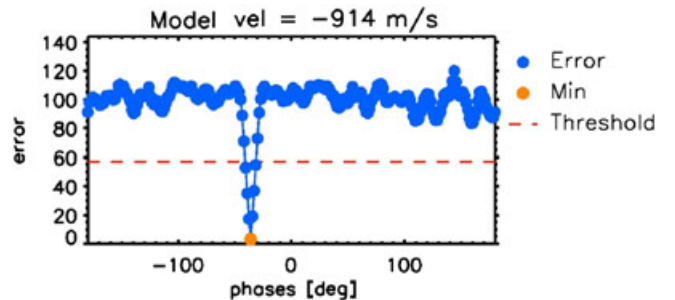
2.3. FITEX2

[15] FITEX2 represents an iteration on an earlier routine called FITEX. FITEX was originally developed as a new method to fit velocity data from a particular pulse sequence,

known as *tauscan*, which is described in *Greenwald et al.* [2008]. Similar to FITACF, a weighted linear least-squares fit to the log of the ACF lag powers is used to resolve SNR and spectral width. However, the phase fitting differs significantly. Instead of the linear phase fit, 120 phase variation models spanning the 180° range at 1.5° intervals are calculated and compared to the phases of the actual data. The number of models used is a trade-off between the computational burden of doing the comparison, which increases with the number of models, and the resolution of the velocity determination. These predetermined models are then fitted to the actual sawtooth pattern (e.g., Figure 3a) without the need for an initial guess on the number of 2π cycles across the ACF lag range. Once this comparison is complete, the model that produces the lowest root-mean-squared (RMS) error is chosen to be the best fit. If this best fit produces an RMS error more than three standard deviations below the mean error across all models, then it is determined that the fit is valid ("good"), and v is calculated from the model. The major disadvantage of FITEX is that it only provides ≈ 25 m/s velocity resolution because of the discrete steps in the phase slopes of the 120 models. The result of the model comparison with the data in Figure 3 is shown in Figure 5.

[16] The subsequent version, FITEX2, was developed to solve Doppler velocity to arbitrary resolution. For improvement of Doppler velocity resolution, the best model phase fit from FITEX is used as an initial guess for the bisection method algorithm described in *Press et al.* [1992]. This provides arbitrary velocity resolution, while only increasing processing time by the equivalent of 5–10 model comparisons. For the data in Figure 3, FITEX2 returns $v = -916$ m/s, $W = 73$ m/s, and SNR = 20 dB, which are essentially the same as determined by FITACF. The FITEX criteria for a good fit are also used in FITEX2.

2.4. LMFIT

[17] In contrast to FITACF and FITEX2, which apply two separate fitting procedures for the ACF phase and power, this routine performs a single model fit to a complex ACF consisting of real and imaginary parts, so that v, w, and SNR are resolved simultaneously. Specifically, R_0, Doppler frequency, and decay time constant are adjusted to fit a

Figure 5. FITEX2 model comparison results for the ACF in Figure 3. The orange circle represents the lowest error model. The horizontal dashed line represents the error threshold for a good model fit (three standard deviations below the mean model error). The model velocity which produces the lowest error is –914 m/s.
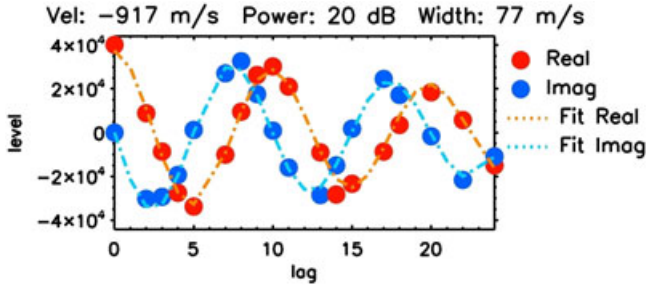
Figure 6. LMFIT results for the ACF in Figure 3. The red and blue circles represent the actual ACF, whereas the orange and blue lines represent the fitted ACF calculated from the outputs of the LMFIT algorithm.

model to the empirical data. Previously, *Ponomarenko et al.* [2008] used this method to fit ACFs in the special case of "mixed scatter," which occurs when a single range gate contains backscatter from two distinct targets, which are usually ionospheric plasma irregularities and the terrestrial surface (ground scatter). It should be noted that in this paper, we are only testing the ability of LMFIT to fit single-component scatter. The name LMFIT is given to this approach because it utilizes the Levenberg-Marquardt nonlinear fitting method [*Levenberg*, 1944; *Marquardt*, 1963; *Press et al.*, 1992].

[18] In order to apply LMFIT, the ACF must be expressed as a single function. We choose to use a modified version of an exponentially decaying harmonic function described by *Ponomarenko et al.* [2008], i.e.,

$$R(\tau) = R_0 e^{-\tau/t_d} e^{j 2\pi \tau f_d}, \tag{4}$$

where $j = \sqrt{-1}$, and $f_d = \frac{1}{2\pi} \frac{\partial \phi}{\partial \tau}$ is the Doppler frequency. In this equation, the first exponential describes the decay of the signal amplitude, while the second (complex) exponential describes the phase variation of the signal. Doppler velocity, spectral width, and SNR (in dB) can then be calculated using equations (5), (3), and (2), respectively.

$$v_d = \lambda f_d / 2. \tag{5}$$

[19] For implementation of the Levenberg-Marquardt algorithm, the free C library MPFIT is used [*Markwardt*, 2009]. This requires that initial guesses be provided on the three parameters before the fitting starts. For this purpose, we used the Doppler velocity and spectral width results from FITEX in order to provide initial guesses of f_d and t_d. The decay time parameter is limited to between 0.001 and 1000 s, which correspond to spectral widths of about 4000 and 0.004 m/s, respectively. Values measured by SuperDARN radars typically range from zero to hundreds of meters per second. The initial guess for R_0 is set to the value of the real part of the ACF at lag zero. A good fit status is returned from LMFIT if (1) the model comparison yields a result with an error that is three standard deviations below the mean model error (as in FITEX2), (2) MPFIT returns a nonerror status, and (3) R_0 is greater than 150% of the ACF error on the fit.
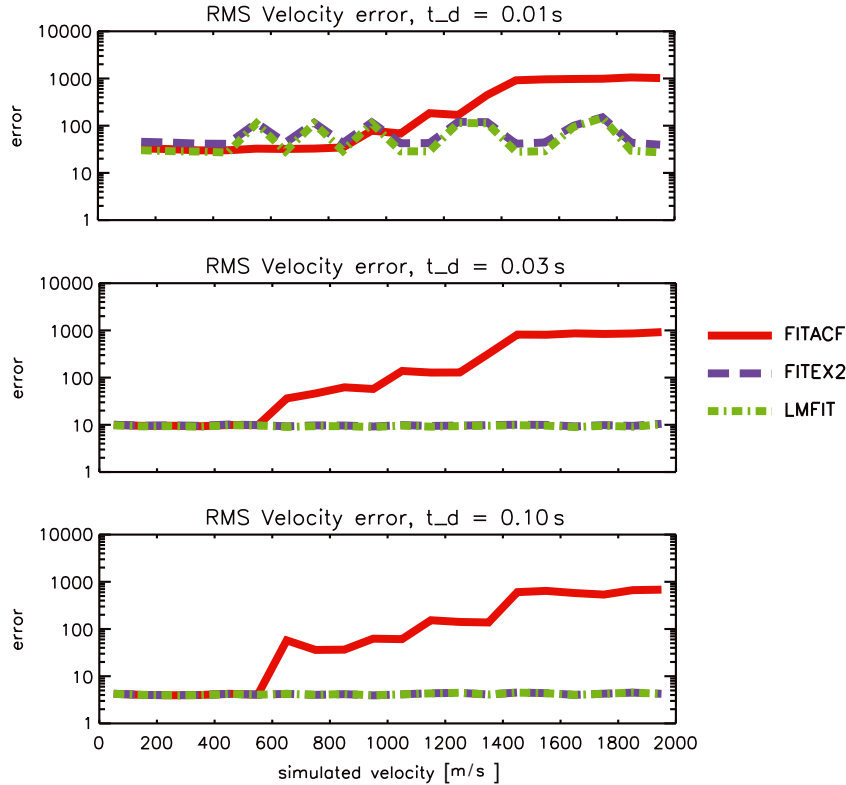
Figure 7. RMS velocity estimate errors for the three fitting routines for three different decay times, 0.01, 0.03, and 0.10 s, which correspond to spectral widths of 398, 133, and 39 m/s, respectively. The *x*-axis shows simulated velocity. The *y*-axis represents RMS errors. The red, purple, and green lines represent FITACF, FITEX2, and LMFIT, respectively.
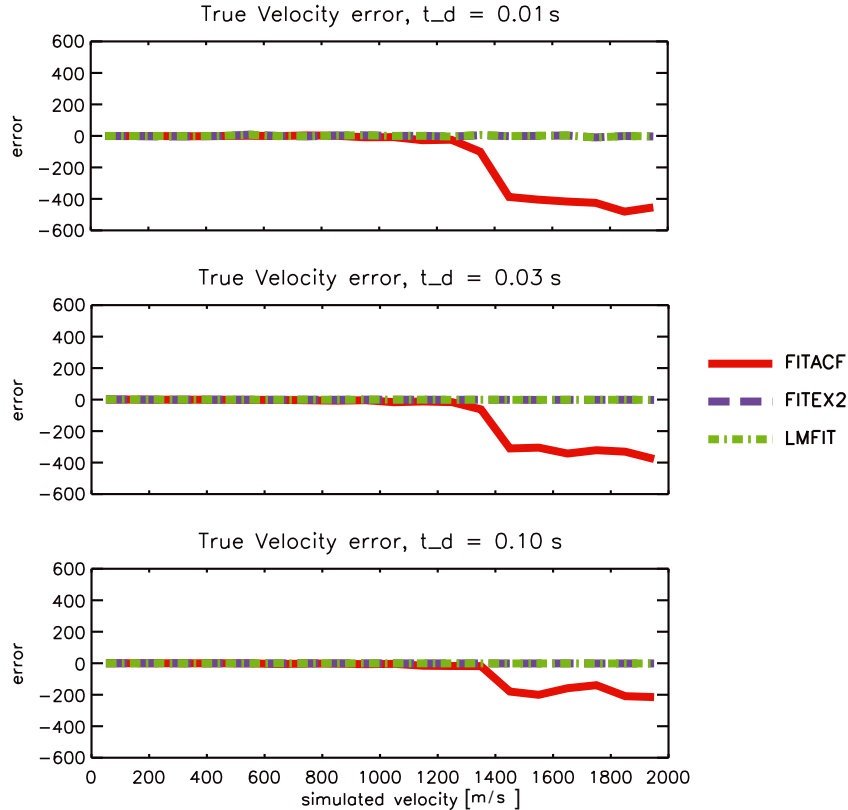
Figure 8. True velocity estimate errors for the three fitting routines for three different decay times organized by simulated velocity. The true error is calculated as fitted velocity minus simulated velocity. The display format is the same as in Figure 7.

ACF error is a measure of how far an ideal ACF generated from the fitted parameters deviates from the ACF being fitted. The result of using LMFIT on the ACF from Figure 3 is shown in Figure 6. LMFIT returns a Doppler velocity of –917 m/s, a spectral width of 77 m/s, and an SNR of 20 dB.

3. Test Data

[20] For thorough testing of all three fitting routines, we used artificial ACFs generated by a simulator described in detail by *Ribeiro et al.* [2013]. The simulator allows us to set desired values for v, t_d (w), and SNR. Importantly, the simulator utilizes the collective scatter approach allowing for realistic simulation of the statistical variability of the backscatter echoes by setting the appropriate number of averaged pulse sequences.

[21] In order to cover a range of v and w, we simulate data over a two-dimensional grid of values with fixed decay time and Doppler velocity at the nodes. We used the eight-pulse sequence *katscan* (Figure 2) with basic lag of τ_0 = 1.5 ms, radar frequency f_0 = 12 MHz and N_{avg} = 35. The simulated data contains Doppler velocity values from 50 to 1950 m/s in 100 m/s steps, and decay time values from 0.01 to 0.1 s in 0.01 s steps. SNR is fixed at a maximum of 25 dB. The effects of irregularity growth, particle precipitation, and velocity spread are set to be negligible in the simulation parameters. There are 500 samples for each combination of decay time and Doppler velocity, resulting in a total of 100,000 ACFs. Note that decay time is referred to

here instead of spectral width because it is the more fundamental value and does not have a linear relation with spectral width. Conversely, Doppler velocity is used even though Doppler frequency is the more fundamental value, because it does have a linear relationship with frequency. In the remainder of this paper, decay time and Doppler velocity will be the values used to address error. Lag zero power error will not be examined because although much information is potentially available from the backscattered power measurement, these data are little used, and we simplify our presentation here by not examining the error on the lag zero power estimate.

[22] In order to simulate a realistic range profile of the backscatter echoes, each integration period contains a band of 10 range gates containing scatter separated by 45 km. The SNR decreases with range R as $1/R^2$ to account plausibly for the geometrical decay of the radar transmission. This coefficient of $1/R^2$ is appropriate for ionospheric beam filling, as opposed to hard target backscatter which would decay as $1/R^4$. Here, $R = (n + 1) \times 45$ km, where $n = 0$–9 is the range gate number.

4. Results

[23] For the comparison, all 100,000 simulated ACFs are fed into the three fitting routines, and the results are stored. Three specific types of error are examined specifically for this exercise, and these will be explained later on in the paper. For all three types, error will be calculated in terms of the deviations from the inputs to the simulator. Regardless of
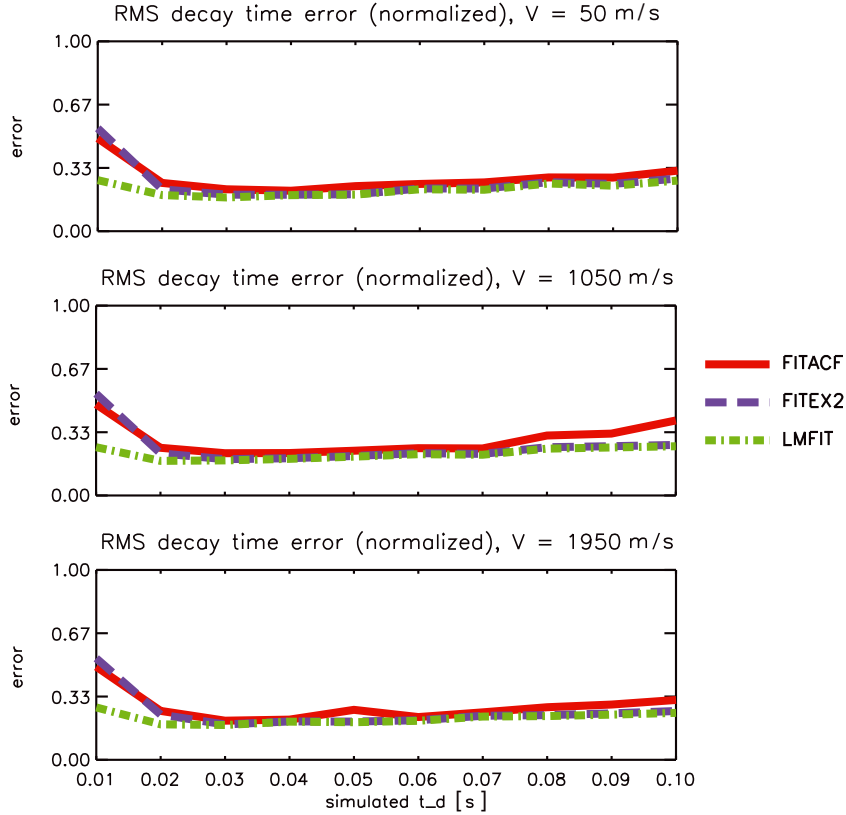
Figure 9. RMS decay time estimate errors for the three fitting routines for three different simulated Doppler velocities. The display format is the same as in Figure 7.

type, error values are only retained for the specific routines which return a good fit.

[24] First, Doppler velocity estimate error is analyzed in a root-mean-squared (RMS) error fashion to review the typical error magnitude, i.e.,

$$\sigma_v = \sqrt{\langle (v - v_0)^2 \rangle}, \qquad (6)$$

where v is the fitted velocity, v_0 is the velocity input to the simulator, and the brackets indicate averaging over all of the valid fitted values. Second, the presence of a regular bias/offset is analyzed in terms of mean (signed) deviation,

$$\Delta_v = \langle v - v_0 \rangle . \qquad (7)$$

[25] Finally, normalized RMS errors are examined for fitted decay times. The errors are calculated in a similar fashion to the velocity errors, except that they are normalized by the original input (to the simulator) decay time quantity, i.e.,

$$\sigma_t = \sqrt{\langle [(t_d - t_{d0})]^2 \rangle}/t_{d0}, \qquad (8)$$

where σ_t is the error on the decay time estimate, t_d is the fitted decay time, and t_{d0} is the decay time input to the simulator. True decay time errors are not discussed in this paper because none of the fitting routines exhibit a bias in the calculation of decay time.

4.1. Velocity Errors

[26] The velocity errors are most important because they have a direct influence on the main SuperDARN product, high-latitude plasma circulation, and electric field

maps which are based on the Doppler velocity estimates [*Ruohoniemi and Baker*, 1998]. Because of this, velocity error should be the primary consideration in determining which fitting method provides the best performance.

4.1.1. RMS

[27] Figure 7 presents σ_v (equation (6)) for three values of input t_{d0} = 0.01, 0.03, and 0.10 s which correspond to $W \approx 398$, 133, and 39 m/s, respectively. The first feature that stands out is that FITACF performs extremely poorly for higher (> 1 km/s) Doppler velocities. Another feature that is apparent is that FITEX2 and LMFIT have some pronounced errors with bad fits at t_{d0} = 0.01 s, i.e., for very wide spectra. These bad fits occur in the same velocity bins because FITEX processing is used to obtain an initial velocity for LMFIT. In general, LMFIT outperforms the other methods for t_{d0} < 0.03 (W > 133 m/s), and all three fitting routines stabilize above this level. Figure 7 also illustrates that with longer decay time (decreasing spectral width), the error in velocity estimates generally decreases for all three methods.

4.1.2. Bias

[28] Another aspect of the velocity estimation that must be examined is whether any of the three fitting routines have a statistical high or low bias, i.e., a chronic underestimation or overestimation of velocity. To illustrate this, in Figure 8, we show mean velocity deviation, Δ_v (equation (7)). Again, three different simulated decay times are pictured, 0.01, 0.03, and 0.1 s. It is immediately apparent that FITEX2 and LMFIT have no apparent bias, while FITACF consistently produces velocities with the wrong sign for $|v| \geq 1000$ m/s. This bias begins when the simulated velocity is high enough

to cause problems with the initial guess of the number of 2π phase cycles. This effect will be discussed later in this paper.

4.2. Decay Time (Spectral Width) Errors

[29] Spectral width is the second most scientifically important parameter that is returned from these fitting routines, as it is typically used in conjunction with Doppler velocity to classify backscatter as ionospheric or ground [*Blanchard et al.*, 2009]. It has also been used as a proxy to estimate the location of the open-closed magnetic field line boundary at auroral latitudes [*Chisham et al.*, 2007].

[30] As was mentioned previously, spectral width error is examined in terms of decay time, because this is the more fundamental parameter in (4). Also, only the RMS error is considered, because none of the three routines exhibit a bias in terms of average true error.

4.2.1. RMS

[31] The results of this comparison can be seen in Figure 9, which shows σ_t (equation (8)) for all three fitting routines. We found that, in contrast to σ_v, the absolute values of RMS decay time errors are approximately proportional to the input t_{d0} value, so we show errors normalized by the respective simulated decay time, t_{d0}. Panels are shown for v_0 = 50, 1050, and 1950 m/s. It is apparent that simulated velocity does not have a strong effect on the quality of the decay time estimates. In general, LMFIT provides better decay time estimates than FITACF and is also noticeably better than FITEX2 for t_d < 0.3 s. None of the three routines, however, exhibit very poor performance.

4.3. Calculation Efficiency

[32] Another factor which must be considered is which fitting routine is more stable and produces a larger percentage of valid fits. After all, a routine might be able to estimate all parameters perfectly, but if it can only fit one out of every 10 ACFs which contain backscatter, then it is essentially useless. In order to test this, again, all three routines were run on the file with the 100,000 simulated ACFs. FITACF produced 99,714 good fits, while FITEX2 and LMFIT both produced 99,703 good fits. The fact that LMFIT and FITEX2 have the same number of fits is a direct result of LMFIT using a FITEX style process for obtaining an initial velocity guess. Regardless of this, all three routines produce a similar number of good fits.

5. Discussion

[33] The major finding of this work is that FITACF velocity fitting is inferior to the other two routines at velocities in excess of 1 km/s. The root of this problem lies in the fact that an initial guess for 2π phase cycles is made. FITACF uses lags 1–4 to make an initial guess on the number of 2π phase jumps to be expected across the entire lag time extent of the ACF. When the velocity magnitude exceeds 1 km/s, the first 2π "flip" occurs within these four lags so that missing one or two lags can lead to a wrong initial guess. This effect is illustrated in Figure 10, which represents phases of two ACFs simulated with the input velocity v = 1750 m/s. In the top panel, only lag one is bad so that FITACF performs an accurate fit and perfectly reproduces the simulated velocity value. In the bottom panel, both lags one and two are bad so that the use of the remaining lags three and four produce
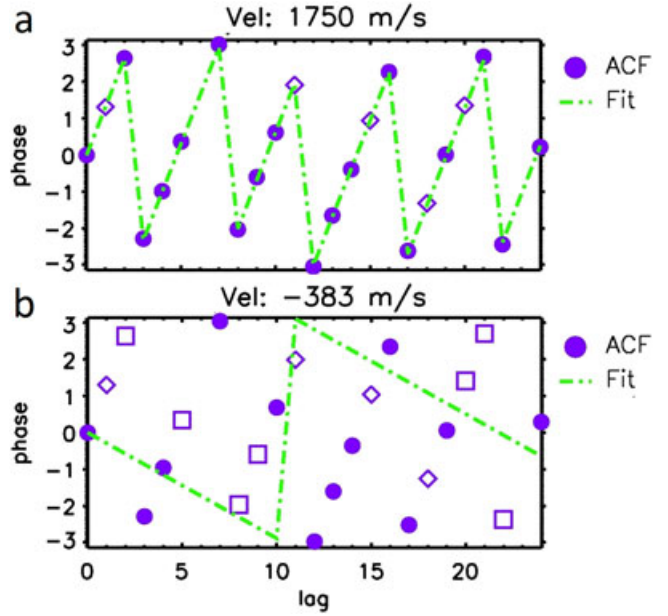
Figure 10. An example of a bad FITACF velocity fit. Figure 10a shows a good phase fit of a simulated ACF with a velocity of 1750 m/s. Figure 10b shows a bad phase fit of a simulated ACF with a velocity of 1750 m/s.

wrong guesses on both the magnitude (generally lower in magnitude) and the sign of the phase slope. Ultimately, this leads to a bad velocity estimate of –383 m/s. As we mentioned before, FITEX2 and LMFIT do not use the four-lag guess procedure, so they are not affected by this artifact.

[34] Another noticeable effect is that the magnitude of the σ_v generally decreases with increasing t_{d0}. This is true of all three fitting routines and occurs because the velocity fitting is sensitive to decay time. As lag power decreases, the statistical fluctuation level σ_P remains constant and makes up a larger portion of the signal level in the ACF, which causes increased uncertainty in the phase fit. This calculation is illustrated in equation (9). Thus, as t_d decreases, the number of lags with lower power increases, resulting in higher uncertainty in the phase fit.

$$\phi(\tau) = \tan^{-1} \frac{Im\{R(\tau)\} \pm \sigma_{Re}}{Re\{R(\tau)\} \pm \sigma_{Im}}. \tag{9}$$

[35] The third significant finding is that, except in the case of FITACF at high velocities, σ_v is independent of the velocity itself. The reason for this is that, while the statistical errors for ACF power depend on power itself, i.e., $\sigma_P = R_0/\sqrt{N_{avg}}$, ACF phase is an arbitrary parameter, so its fluctuations cannot depend on the phase magnitude. In fact, they are also determined by the ACF power (more specifically, correlation coefficient) at a given lag [*Bendat and Piersol*, 1986]. Therefore, theoretically, one would not expect to observe velocity magnitude effects on statistical fluctuations of any estimated parameters, including t_d.

[36] Conversely, σ_t is fairly constant across all tested values of t_{d0}. The proportionality of nonnormalized decay time errors, σ_d, to t_{d0} can be illustrated using the propagation of ACF power errors onto decay time. In estimating t_d, we are looking for a point on the time lag axis which corresponds

Table 1. Fitting Method Performance Summary

	FITACF	FITEX2	LMFIT
Number of fits	99,714	99,703	99,703
Median v_d error (m/s)	4.855	4.646	4.526
Mean v_d error (m/s)	91.42	8.447	7.291
Median t_d error (norm.)	0.1591	0.1591	0.1453
Mean t_d error (norm.)	0.2124	0.2056	0.1755

to the e-fold decay of ACF power. The propagation of errors method gives us a respective decay time uncertainty, $\sigma_d = \sigma_P \left| \frac{\partial t_d}{\partial R} \right|$. We are interested in the decay time error at $\tau = t_d$. With changing t_d, the power uncertainty, σ_P, remains essentially constant, but the derivative term (inverted slope of $P(\tau)$ at $\tau = t_d$) increases or decreases proportionally so that $\sigma_d \propto t_d$. Detailed theoretical analysis of statistical fluctuations lies beyond the scope of this manuscript, but we plan to address it in a future paper.

[37] Table 1 presents a summary of the performance characteristics of all three fitting routines. Note that some of the errors presented here have been normalized by the simulated parameters. For example, a normalized decay time error is calculated as $|t_0 - t| / t_0$. Mean and median errors are shown for velocity and decay time. In both median and mean comparisons, LMFIT has the lowest errors for all fitted parameters. Although several of the results are very close, the results are unanimous. The sole weakness of LMFIT is a longer run time. Future work could focus on developing a new method of providing LMFIT with an initial velocity guess in order to sever the tie to FITEX, possibly eliminating the bad fits seen in the top panel of Figure 7.

6. Summary and Conclusions

[38] After examination of the error characteristics and effectiveness at extracting estimates from ACFs, we conclude that LMFIT is the fitting routine which generally performs best in estimating ionospheric parameters on the basis of SuperDARN radar measurements. The conventional routine FITACF performs very well at $|v| \le 1000$ m/s, but at higher velocities, eventual data contamination at the shortest lags causes it to produce systematically poor estimates. In sum, LMFIT significantly outperforms FITACF and slightly outperforms FITEX2. Finally, we note that the findings and routines reported here are applicable to other multipulse radar systems that have been designed to overcome the range ambiguity/velocity aliasing dilemma.

References

Baker, K. B., J. R. Dudeney, R. A. Greenwald, M. Pinnock, P. T. Newell, A. S. Rodger, N. Mattin, and C. I. Meng (1995), HF radar signatures of the cusp and low-latitude boundary layer, *J. Geophys. Res.*, *100*(A5), 7671–7695.

Barthes, L., R. André, J. C. Cerisier, and J. P. Villain (1998), Separation of multiple echoes using a high-resolution spectral analysis for SuperDARN HF radars, *Radio Sci.*, *33*(4), 1005–1017.

Bendat, J. S., and A. G. Piersol (1986), *Random Data. Analysis and Measurement Procedures*, John Wiley & Sons, Inc., New York, Chichester, Brisbane, Toronto and Singapore.

Blanchard, G. T., S. Sundeen, and K. B. Baker (2009), Probabilistic identification of high-frequency radar backscatter from the ground and ionosphere based on spectral characteristics, *Radio Sci.*, *44*(5), RS5012, doi:10.1029/2009RS004141.

Chisham, G., et al. (2007), A decade of the Super Dual Auroral Radar Network (SuperDARN): Scientific achievements, new techniques and future directions, *Surv. Geophys.*, *28*(1), 33–109, doi:10.1007/s10712-007-9017-8.

Farley, D. (1972), Multiple-pulse incoherent-scatter correlation function measurements, *Radio Sci.*, *7*(6), 661–666.

Greenwald, R. A., K. B. Baker, R. A. Hutchins, and C. Hanuise (1985), An HF phased-array radar for studying small-scale structure in the high-latitude ionosphere, *Radio Sci.*, *20*(1), 63–79.

Greenwald, R. A., K. Oksavik, R. Barnes, J. M. Ruohoniemi, J. Baker, and E. R. Talaat (2008), First radar measurements of ionospheric electric fields at sub-second temporal resolution, *Geophys. Res. Lett.*, *35*, L03111, doi:10.1029/2007GL032164.

Hanuise, C., J. P. Villain, D. Gresillon, B. Cabrit, R. A. Greenwald, and K. B. Baker (1993), Interpretation of HF radar ionospheric Doppler spectra by collective wave scattering theory, *Annales Geophysicae*, *11*(1), 29–39.

Lehtinen, M. S. (1986), Statistical theory of incoherent scatter measurements, Univ. of Helsinki, Ph.D. thesis, Helsinki, Finland.

Levenberg, K. (1944), A method for the solution of certain problems in least squares, *Quart. Applied Math.*, *2*, 164–168.

Markwardt, C. B. (2009), Non-linear least-squares fitting in IDL with MPFIT, *Astron. Soc. Pac. Conf. Ser.*, *411*, 251–254.

Marquardt, D. W. (1963), An algorithm for least-squares estimation of nonlinear parameters, *J. Soc. Ind. Appl. Math.*, *11*(2), 431–441.

Ponomarenko, P. V., and C. L. Waters (2006), Spectral width of SuperDARN echoes: Measurement, use and physical interpretation, *Ann. Geophys.*, *24*(1), 115–128, doi:10.5194/angeo-24-115-2006.

Ponomarenko, P. V., C. L. Waters, and F. W. Menk (2007), Factors determining spectral width of HF echoes from high latitudes, *Ann. Geophys.*, *25*, 675–687, doi:10.5194/angeo-25-675-2007.

Ponomarenko, P. V., C. L. Waters, and F. W. Menk (2008), Effects of mixed scatter on SuperDARN convection maps, *Ann. Geophys.*, *26*(6), 1517, doi:10.5194/angeo-26-1517-2008.

Press, W. H., S. A. Teukolsky, W. T. Vetterling, and B. P. Flannery (1992), *Numerical Recipes in C: The Art of Scientific Computing*, 2nd edn., pp. 350–354 and 683–687, Cambridge University Press, New York, NY.

Ribeiro, A. J., P. V. Ponomarenko, J. M. Ruohoniemi, J. B. H. Baker, L. B. N. Clausen, R. A. Greenwald, and S. de Larquier (2013), A realistic radar data simulator for the Super Dual Auroral Radar Network, *Radio Sci.*, doi:10.1002/rds.20032.

Ruohoniemi, J. M., and K. B. Baker (1998), Large-scale imaging of high-latitude convection with Super Dual Auroral Radar Network HF radar observations, *J. Geophys. Res.*, *103*(A9), 20797–20811, doi:10.1029/98JA01288.

Uppala, S. V., and J. D. Sahr (1994), Spectrum estimation of moderately overspread radar targets using aperiodic transmitter coding, *Radio Sci.*, *29*(3), 611–623.